Demonstration of a Shell-Core Structure in Layered CdSe-ZnSe Small Particles by X-ray Photoelectron and Auger Spectroscopies

Carolyn F. Hoener, Kristi Ann Allan, Allen J. Bard, Alan Campion, Marye Anne Fox,* Thomas E. Mallouk, Stephen E. Webber, and J. M. White

Department of Chemistry, University of Texas at Austin, Austin, Texas 78712 (Received: December 2, 1991; In Final Form: January 17, 1992)

The preferential positioning of different cations near the surface or at the center of small layered CdSe-ZnSe particles believed to have a shell-core structure has been demonstrated by the relative attenuation of the primary photoelectron and X-ray excited Auger signals from each cation. The preparation of the layered particles is described, and their absorption spectra are compared with those observed in "unstructured" particles of like composition.

Introduction

The optical absorption onsets of small semiconductor particles (up to 100 Å in diameter) occur at higher energies than those of the bulk materials.[1] The largest particle in which such a blue-shift can be observed is roughly the same size as an exciton. One rationalization for the observed blue-shift is that since the excitations of a particle are spatially confined to its dimensions, an exciton on a particle which is smaller than a bulk exciton must be compressed, thus raising the transition energy and shifting the absorption onset to higher energy. An approximate model for the lowest excited states of such a particle is the solution to the particle-in-a-sphere problem.[2,3] An alternate description of the same phenomena can be ascribed to reduced mixing of atomic orbitals (leading to delocalization) deriving from the small number of atoms in these particles. The smaller number of atoms also leads to incomplete development of band structure with discrete energy levels. At some point, as the particle size decreases, the electronic structure of the system is better described by a molecular picture.

"q-particles" (so-called because they exhibit "quantum confinement") are small particles in which blue-shifted absorption onsets are observed. They can be prepared in various media: glasses,[4] zeolites,[5-7] ion-exchange membranes,[8-10] and inverse micelles.[11-14] These preparation techniques differ with respect to interactions with the host media, range and distribution of particle sizes, long-term stability, and accessibility to solution species. Preparation of small particles within inverse micelles provides a narrow particle size distribution, which facilitates spectroscopic characterization, but the resulting particles lack long-term stability. Recently, schemes have been developed to stabilize particles grown in inverse micelles by surface modification,

e.g., "capping"[15,16] by organic thiols or selenols. An additional benefit of this treatment is that it allows the particles to be separated from the micellar solution and redispersed in another solvent.

Many experiments[3,4,12,17,18] have been devised to improve our understanding of the changes which take place in the electronic and optical properties of small semiconductor particles as the particle size is decreased. Once these effects and their origins are understood, they may serve as powerful tools in selecting and designing photocatalysts. One such sample type expected to aid in the investigation of these changes consists of layered particles in which a core "Q-particle" is spatially insulated, and its surface states are passivated, by a surrounding shell of a wider band gap material.

Recently, the synthesis of layered CdSe-ZnS particles has been reported.[19] However, despite reasonable assumptions, this report failed to demonstrate unambiguously that a shell-core structure (Figure 1a) had been obtained. This structure could not be established by X-ray diffraction patterns because the core sizes were too small. A comparison of the sample's overall atomic composition to the ratio of the observed Cd and Zn Auger peak heights in particles with CdSe and with ZnS cores revealed a greater than expected attenuation of the electrons emitted from the shell material. This result implies that the core material had a greater surface concentration than expected from a symmetrical shell-core model and suggests the possibility that particles of the "shell" material might have grown separately or on only part of the surface of the core particle, as illustrated in Figure 1b. Alternatively, the apparent contradiction may have been caused by the effects of particle composition and structure on the electron mean free paths or other matrix effects in these materials.

The objective of the work reported herein is to demonstrate a shell-core structure in analogous CdSe-ZnSe layered particles. In a perfectly symmetrical "shell-core" particle, the core material would be completely buried under a uniform layer of the shell material. If the thickness of this shell were 4-12 Å, X-ray photoelectron spectroscopy (XPS) and X-ray excited Auger

(1) Brus, L. E. *J. Phys. Chem.* **1986,** *90,* 2555.

(2) Brus, L. *J. Chem. Phys.* **1984,** *80,* 4403.

(3) Chestnoy, N.; Hull, R.; Brus, L. E. *J. Chem. Phys.* **1986,** *85,* 2237.

(4) Ekomov, A. I.; Efros, A. L.; Onushchenko, A. A. *Solid State Commun.* **1985,** *56,* 90.

(5) Wang, Y.; Herron, N. *J. Chem. Phys.* **1987,** *91,* 257.

(6) Herron, N.; Wang, Y.; Eddy, M. M.; Stucky, G. D.; Cox, D. E.; Bein, T. *J. Am. Chem. Soc.* **1989,** *111,* 530.

(7) Moller, K.; Bein, T.; Eddy, M. M.; Stucky, G. D.; Herron, N.; Wang, Y.; Cox, D. E. *NSLS Annu. Rep.* **1988,** 247.

(8) Krishnan, M.; White, J. R.; Fox, M. A.; Bard, A. J. *J. Am. Chem. Soc.* **1982,** *105,* 7002.

(9) Dimitrijevic, N. M.; Kamat, P. V. *J. Phys. Chem.* **1987,** *91,* 2096.

(10) Kuczynski, J. P.; Milosaljevic, B. H.; Thomas, J. K. *J. Phys. Chem.* **1984,** *88,* 980.

(11) Petit, C.; Pileni, M. P. *J. Phys. Chem.* **1988,** *92,* 2282.

(12) Meyer, M.; Wallberg, C.; Kurihara, K.; Fendler, J. H. *J. Chem. Soc., Chem. Commun.* **1984,** 90.

(13) Dannhauser, T.; O'Neil, M.; Johansson, K.; Whitten, D.; McLendon, G. *J. Phys. Chem.* **1986,** *90,* 6074.

(14) Lianos, P.; Thomas, J. K. *Chem. Phys. Lett.* **1986,** *125,* 299.

(15) Herron, N.; Wang, Y.; Eckert, H. *J. Am. Chem. Soc.* **1990,** *112,* 1322.

(16) Steigerwald, M. L.; Alivisatos, A. P.; Gibson, J. M.; Harris, T. D.; Kortan, R.; Muller, A. J.; Thayer, A. M.; Duncan, T. M.; Douglass, D. C.; Brus, L. E. *J. Am. Chem. Soc.* **1988,** *110,* 3046. Note that the designations for the shell and core material used in ref 16 are inverse to those adopted in this article.

(17) Alivisatos, A. P.; Harris, T. D.; Carroll, P. J.; Steigerwald, M. L.; Brus, L. E. *J. Chem. Phys.* **1989,** *90,* 3463.

(18) Alivisatos, A. P.; Harris, A. L.; Levinos, N. J.; Steigerwald, M. L.; Brus, L. E. *J. Chem. Phys.* **1988,** *89,* 4001.

(19) Kortan, A. R.; Hull, R.; Opila, R. L.; Bawendi, M. G.; Steigerwald, M. L.; Carroll, P. J.; Brus, L. E. *J. Am. Chem. Soc.* **1990,** *112,* 1327. Bancroft, G. M.; Adams, I.; Lampe, H.; Shaw, T. K. *J. Electron Spectrosc.* **1976,** *9,* 191.
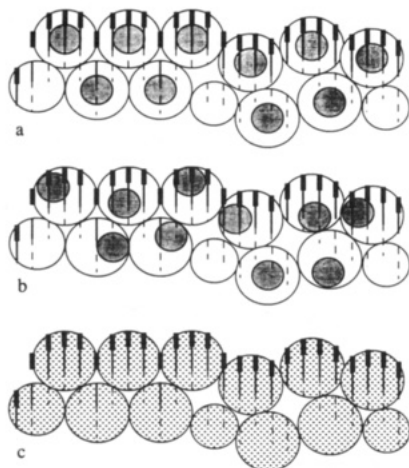
Figure 1. Models for pressed powders of composite particles: (a) particles with the desired shell–core structure; (b) particles in which the "shell" material does not surround the core so that the distribution of the materials appears random at all depths; (c) particles without ordered cation random distribution of the two component materials. The thick lines indicate regions near the surface from which the probability of detecting emitted electrons is the greatest.

spectroscopy, techniques whose surface sensitivities lie in this range, might reasonably be used to demonstrate layering. X-ray excitation is used to create core holes by the emission of electrons with kinetic energies characteristic of the excited atoms (roughly, the excitation energy less the binding energy of the emitted electron). The resultant core holes are filled with electrons from higher lying occupied orbitals, an exoenergetic process. One way the energy from this process is released is by the emission of Auger electrons. The depth dependence of the observed signal intensity, I, for the Auger and the primary X-ray photoemitted electrons is

$$I = I_0 e^{-z/\lambda} \qquad (1)$$

where z is the distance of the emitting atoms from the sample surface, I_0 is the unattenuated signal intensity, and λ is the (energy- and material-dependent) attenuation length of the emitted electron. The probability of detecting a photoelectron from an atom buried in the material is significantly smaller than from an atom near the surface. As long as the mean free path for the emitted electron is not much larger than z, this provides a method for testing for the occurrence of the shell–core structure.

In this paper, the preparation and characterization of two types of constant-composition CdSe–ZnSe particles, presumed to have a random and a shell–core structure, are described. The synthesis is similar to that previously reported for CdSe–ZnS composite particles.[19] The relative signal intensities of the XPS and Auger electrons emitted by the Cd and Zn cations in these samples are compared to those in particles of similar atomic composition, as determined by energy dispersive X-ray spectroscopy (EDS), which were prepared with no attempt to control the spatial distribution of the cations. This comparison demonstrates that the expected shell–core structure is present, i.e., that the material intended to be localized in the shell is indeed concentrated near the surface and that the material intended as the core is indeed buried in the synthetic layered particles. Evidence of a strong dependence of the electron attenuation lengths on the overall particle composition is seen, and the ultraviolet–visible absorption spectra of the structurally characterized particles are presented and discussed.

Experimental Section

Water was purified by filtration with a Millipore "Milli-Q" system (Continental Water Systems, El Paso, TX). Cadmium perchlorate (99.9%) and zinc perchlorate (98.9%) (Alfa), benzeneselenol, methyllithium, chlorotrimethylsilane, and "super-hydride" (lithium triethylborohydride in THF) (Aldrich), and selenium powder (99.9%, Aesar Johnson Matthey Inc.) were used as received. All solvents were analytical reagent grade and were used as received except heptane, which was degassed with argon,

and pyridine, which was dried over KOH and distilled before use.

Dioctylsulfosuccinate sodium salt (AOT) was obtained from Alfa, dissolved in petroleum ether, filtered, and dried under argon to remove impurities and oxygen. A stock solution of 55.5 mM AOT in heptane was prepared, such that W (= moles of water/moles of surfactant) of inverse micelles made from this stock was equal to the number of milliliters of aqueous solution used per liter of AOT solution. Bis(trimethylsilyl) selenide (bisTMS-Se)[20] and phenyltrimethylsilyl selenide (PhTMS-Se),[21] synthesized by literature procedures, were prepared as stock solutions, 0.02 and 0.03 mM respectively, and stored cold (for less than 48 h). Aqueous 1 M stock solutions of $Cd(ClO_4)_2$ and $Zn(ClO_4)_2$ were degassed and stored under Ar.

Capped particles were prepared by the method of Steigerwald et al.[16] The particles were grown in inverse micelles with aqueous phases consisting of <1 M $M(ClO_4)_2$ solution (where $M = Cd^{2+}$ or Zn^{2+}). To the micelle solutions (5×10^{-4} to 10^{-3} M overall in cation) was introduced bisTMS-Se as a source of Se^{2-}, to initiate the growth of MSe.

Capped layered particles were prepared by a modification of this method. First, the core particles were grown to a size determined by the initial water-to-surfactant mole ratio, W_1. After the growth of the core particles, the cation from which the second layer was to be grown was added in a micellar solution of larger W, W_2. When the micelles equilibrated, the final water-to-surfactant ratio, W_f (and hence the particle size-determining water pool size), was the average of W_1 and W_2 weighted by the volume of each micellar solution used. Additional bisTMS-Se was added to the resulting micellar solution to initiate deposition of the second material around the core particles. After the growth of the second layer, these particles were capped as described above.

When capped with thiophenyl groups, the particles became insoluble in both the aqueous and organic phases of the micellar solution and precipitated. The particles were washed repeatedly with petroleum ether, dissolved in pyridine, and filtered to remove any large particles. The pyridine was removed under rotary evaporation, and the resulting particles were rinsed in petroleum ether a few more times. The final product was a free flowing powder (65–85% yield).

The resulting capped particles could be redispersed in pyridine. The optical absorption spectra of the particles in pyridine, referenced to a solvent blank, were recorded on a Hewlett-Packard Model 8451A single-beam diode array spectrometer. The low-temperature heating during removal of solvent may have partially annealed the samples: thus, for uniformity, all spectra presented are for particles annealed by heating in refluxing pyridine under Ar for about 1 h.

For the XPS measurements, the powders were pressed into indium foil which was wrapped about an aluminum support. These samples were loaded into a Leybold Heraeus LHS-12 surface analysis system. The XPS system[22,23] was equipped with a dual X-ray anode (Mg and Al) and an EA-11 hemispherical analyzer. A base pressure of 1.5×10^{-9} Torr was maintained during measurement. The X-ray photoelectron spectra were recorded at a collection angle normal to the surface. The data were obtained with Mg $K\alpha$ radiation (1253.6 eV) at 200 W (10 keV, 20 mA) and a 40 eV pass energy, which gave an overall energy resolution of 0.95 eV. The measured kinetic energies were referenced to the C(1s) peak for the phenyl carbons at 969.0 eV.[24]

The atomic composition of the particles was determined by energy dispersive X-ray spectroscopy (EDS) performed on a Jeol JSM-35C scanning electron microscope. CdSe (99.999%, Alfa) and ZnSe (99.99%, Aldrich) were used, as received, as standards. The measured sensitivities of Cd and Zn relative to Se in the

(20) Detty, M. R.; Seidler, M. D. *J. Org. Chem.* **1982**, *47*, 1354.
(21) Liotta, D.; Paty, P. B.; Johnston, J.; Zima, G. *Tetrahedron Lett.* **1978**, 5091.
(22) Allan, K.; Zaou, K.; Goodenough, J.; Campion, A. *Phys. Rev. B*, in press.
(23) Akhter, S.; Allan, K.; Buchanan, D.; Cook, J. A.; Campion, A.; White, J. M. *Appl. Surf. Sci.* **1988/89**, *35*, 241.
(24) Swift, P. *Surf. Interface Anal.* **1982**, *4* (2), 47.

standards were used to determine a Cd/Zn atomic ratio for these samples.

Results and Discussion

Although the precise size of a reagent grown within a reverse micelle depends on both reagent concentration and the water-to-surfactant mole ratio, W, the micellar radius does provide a rough estimate of included particle size. Thus, the semiconductor particles are assumed to have grown to approximately the same size as the water pools of the micelles in which they were prepared. This is determined in turn by W, which is essentially a ratio of the water volume to interface surface area and, thus, is roughly proportional to the micelle's radius. A more precise relationship between W and the radius of the micelle water pool (found to be in good agreement with results obtained in light scattering experiments) is given in eq 2.[25]

$$[(r + 15)/r]^3 - 1 = 27.5/W \qquad (2)$$

This study focuses on layered particles with a 7:1 mole ratio of the shell and core materials. The values of W used were 1.2 for the core and 4.4 overall, corresponding to radii of 8 and 16 Å, respectively. Reference samples with the same overall size (W = 4.4) were prepared with one growth period in micelles containing both cations. It is assumed that this procedure produces particles with a uniform, random cation distribution.

The proportions of the various reagents used were calculated as follows. A quantity x (proportional to the number of particles) was defined as the number of millimoles of the first cation/r_1^3. The first addition of bisTMS-Se produced only $[x(r_1 - 1.5)^3]$ millimoles of Se^{2-}, to assure a cation-rich surface. (A more uniform size distribution is achieved when the particles are kept cation rich.[14]) For layered particles, the second micellar solution containing $[x(r_f^3 - r_1^3)]$ millimoles of the second cation was added with enough bisTMS-Se to bring total millimoles of Se^{2-} to $[x(r_f - 1.5)^3]$, where r_1 and r_f are the water pool radii corresponding to W_1 and W_f. When the particles were capped with phenyl selenide, the number of millimoles of PhTMS-Se required was twice the difference between the number of millimoles of cations and anions added to this point. The same number of millimoles of pyridine was also added to aid in precipitation.

Two pairs of samples were prepared: in one pair, the core of the shell–core particles and the minor component in the unstructured particles were CdSe; in the other pair, ZnSe played these roles. These samples are designated by the following notation:[16] $(MsSe)_7McSe$ is a shell–core sample in which McSe is the core and MsSe the shell material, and Ms_7McSe_8 is a randomly dispersed sample for which no measures were taken to control the locations of the cations.

The 7:1 mole ratio was chosen as a compromise. A thicker shell would provide larger attenuation/amplification effects of the XPS signals, but at the expense of reasonable signal-to-noise for the XPS signals from the core component. The "unstructured" particles are used for standards representing a uniform distribution of cations of the same overall composition into the sample. If the two materials precipitated separately, the X-ray photoelectron spectra sampled over a relatively large area would show a uniform distribution of the cations into the mixture. Because of the low (1:7) mole ratio employed, a close-to-uniform cation distribution with sample penetration depth (Figure 1b) would be observed over a large sample area if the shell material had grown on the surface but not all the way around the core. On the other hand, the electron spectra of samples with a symmetrical shell–core structure (which concentrates certain cations near and others far form the surface, Figure 1a) should show an attenuation of the signals from buried cations and an amplification of the signals from the cations concentrated on the surface, relative to the signal intensities of the unstructured samples.

The direct use of the XPS and Auger signal intensities to determine the particle's structure requires precise knowledge of the particle's composition, the electron attenuation lengths of each
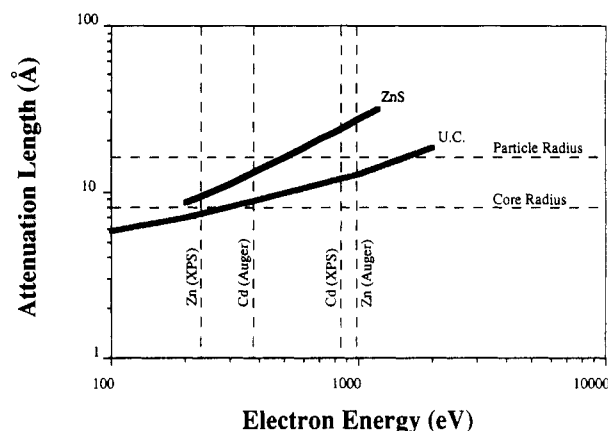
(25) Zulauf, M.; Eicke, H.-F. *J. Phys. Chem.* **1979**, *83*, 480.

Figure 2. Relationship between the kinetic energy of the emitted electrons and their escape depth in the Mg Kα region. The general "universal curve" (UC)[28] and a relationship calculated for ZnS[26] are plotted. The energies of the XPS and Auger electrons emitted by Cd and Zn and the assumed radii of the particle and its core are indicated. Both Cd and Zn emit electrons with smaller attenuation lengths than the assumed radius of the particles.

cation, the incident X-ray flux, and the excitation and emission cross sections for each electron. The electron attenuation length, λ, is a function of the kinetic energy of the electron and the attenuating material. In the region of interest, lower energy electrons have shorter λ; all electrons, particularly those with low energies, are attenuated more by materials with higher average atomic weights.[26] Electron emission cross sections and inelastic mean free paths are not known accurately, in general, and not known at all for unusual materials such as the composites used in this study. In this paper, we therefore assume that the λ values for electrons in particles with a shell–core structure are identical to those for unstructured samples of the same composition.

In this analysis, the need to know the X-ray flux, excitation cross sections, and number of emitting atoms is avoided by comparing the relative intensities of two different characteristic electrons emitted by each cation, Cd and Zn. Both have strong primary photoelectron and Auger signals in the Mg Kα region (180–1253.6 eV). The kinetic energies of the primary photoelectrons of Cd(3d) and Zn(2p) are 849 and 232 eV; the kinetic energies of the Auger electrons are 375 and 990 eV for Cd-$(M_4N_{45}N_{45})$ and Zn$(L_3M_{45}M_{45})$, respectively.[27] For both Zn and Cd, the emitted electrons are widely spaced in energy and hence have significantly different attenuation lengths.

Figure 2 shows the relationship between the kinetic energy of the emitted electrons and their attenuation lengths, in the Mg Kα region. The general "universal curve"[28] and a relationship calculated with Penn's algorithm for ZnS[26] are plotted. The curves for $Cd_xZn_{1-x}Se$ composite materials are expected to be steeper and have lower y intercepts than the calculated ZnS curve, since the effect of the larger average atomic weight, which decreases the attenuation length, is stronger for the lower energy electrons. The energies of the XPS and Auger electrons emitted by Cd and Zn and the assumed radii of the particle and its core are marked in Figure 2. Both Cd and Zn emit electrons with attenuation lengths smaller than the estimated radius of the particles. The low-energy electron signal is attenuated over a shorter distance and therefore is more sensitive to the placement of the atoms relative to the surface of the sample than the high-energy signal. This suggests that the attenuation of the lower energy electron signal relative to that of the higher energy electron can be used to indicate a shell–core structure.

Factors such as the number of atoms, the X-ray flux, and the excitation cross sections which are reflected in the electron signal

(26) Tanuma, S.; Powell, C. J.; Penn, D. R. *Surf. Interface Anal.* **1988**, *11*, 577.
(27) Briggs, D.; Seah, M. *Practical Surface Analysis*; John Wiley & Sons: Chichester, 1988; pp 477–509 and references therein.
(28) Seah, M. P.; Dench, W. P. *Surf. Interface Anal.* **1979**, *1*, 2.

TABLE I: Integrated Areas of the Observed XPS and Auger Signals for Cd and Zn in Unstructured[a] and Layered[b] Small CdSe–ZnSe Particles

electron	$Zn_7CdSe_8{}^a$	$(ZnSe)_7CdSe^b$	$Cd_7ZnSe_8{}^a$	$(CdSe)_7ZnSe^b$
		XPS		
Cd $3d_{3/2+5/2}$ at 842 + 849 eV	1050 ± 10	2780 ± 40	12100 ± 50	7340 ± 50
Zn $2p_{3/2}$ at 232 eV	3840 ± 10	7170 ± 10	830 ± 90	136 ± 9
		Auger		
Cd $M_5N_{45}N_{45}$ at 375 eV	1010 ± 100	1540 ± 50	5800 ± 100	4980 ± 100
Zn $L_3M_{45}M_{45}$ at 990 eV	5240 ± 30	6640 ± 20	1380 ± 10	650 ± 20
		EDS		
Cd/Zn (atomic ratios)	0.19	0.21	9.0	11.5

[a] Ms_7McSe_8 refers to a sample for which no measures were taken to control spatially the locations of the cations. [b] $(MsSe)_7McSe$ refers to a sample with a shell–core structure in which McSe is the core material and MsSe is the shell material.
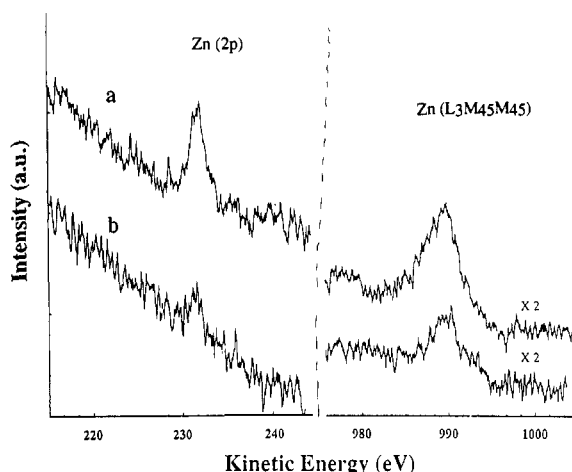

Figure 3. Signals for the primary and Auger electrons emitted by X-ray excited Zn atoms in (a) "unstructured" composite particles with roughly 7 times as much CdSe as ZnSe and (b) particles of the same composition with a shell–core structure (ZnSe core surrounded by CdSe).

intensities are eliminated by ratioing the signal intensities of two electrons emitted by the same element. The other factors buried in the I_0 term of eq 1 (emission quantum yields and instrument response) are eliminated by comparing the relative signal intensities of each shell–core sample to those of an unstructured sample of the same composition; see the Appendix. When the ratio of the signal intensities of the low- and high-energy electrons is divided by the same ratio for an unstructured sample of the same composition, amplification (>1) and attenuation (<1) factors are obtained. These factors for the cations in the shell and core materials are then used to demonstrate spatial layering in the shell–core structure without the need for the exact values of λ.

Figure 3 compares the observed signals for the XPS and Auger electrons emitted by X-ray excited Zn metal ions in Cd_7ZnSe_8, an unstructured composite particles composed of roughly 7 times as much CdSe as ZnSe (top trace) with those for $(CdSe)_7ZnSe$, particles of the same composition in which the ZnSe is buried in the particle core (lower trace). Both signals are smaller in the lower trace than in the upper one. However, there is a greater change in the XPS signal (232 eV) than the Auger signal (990 eV). This difference is caused by attenuation in the CdSe shell which is more rapid for the lower energy electron. This difference in relative signal intensities is indicative of a shell–core structure.

The integrated areas of the XPS and the Auger signals of Cd and Zn are given in Table I, along with the experimental sample compositions. In all cases, the Cd-to-Zn ratio is slightly higher than expected from the synthesis mole ratio. Similar observations have been made for the CdSe ZnS system.[19] The observed experimental mole ratios suggest that the shell–core sample with CdSe on the outside has a slightly thicker shell than that having a ZnSe shell.

The relative signal intensities of the low- and high-energy electrons emitted by Cd and Zn in capped unstructured q-particles are compared to those from powdered bulk CdSe and ZnSe in Table II. In pure CdSe, the signal intensity ratio for the low-

TABLE II: Signal Intensity Ratios for the Low- and High-Energy Electrons Emitted from Both Cd and Zn in Unstructured Materials of Various Compositions

	CdSe	Cd_9ZnSe_{10}	$CdZn_{5.25}Se_{6.25}$	ZnSe
Cd (XPS/Auger)	0.155 ± 0.005	0.17 ± 0.01	0.4 ± 0.1	
Zn (Auger/XPS)		2.6 ± 0.4	2.9 ± 0.1	4.6 ± 0.1

TABLE III: Calculated and Experimental Relative Intensities of the Low- and High-Energy Electrons Emitted by the Cations in Shell–Core Composites[a] Divided by the Relative Intensities Observed in Unstructured Particles[b] of Similar Composition

	$(ZnSe)_7CdSe^a/$ $Zn_7CdSe_8{}^b$	$(CdSe)_7ZnSe^a/$ $Cd_7ZnSe_8{}^b$
	Calculated	
core/minor	0.56	0.30
shell/major	1.09	1.05
	Experimental	
core/minor	0.58 ± 0.06	0.35 ± 0.05
shell/major	1.47 ± 0.01	1.42 ± 0.04

[a] $(MsSe)_7McSe$ refers to a sample with a shell–core structure in which McSe is the core material and MsSe is the shell material. [b] Ms_7McSe_8 refers to a sample for which no measures were taken to control spatially the locations of the cations.

and high-energy electrons emitted by Cd is 0.535 ± 0.005; similar ratios are observed for the Cd signals from capped composite particles. In pure ZnSe, the signal intensity ratio for the low- and high-energy electrons emitted by Zn (3.2 ± 0.1) is significantly higher than that observed for capped composite particles. The observed variation in relative signal intensity emphasizes the need for a well-chosen reference.

A crude model (detailed in the Appendix) was used to estimate the amplification and attenuation factors expected in particles with a uniform shell thickness and core particle radius of $1/2 r$, where r is the radius of the overall particle. The random samples are assumed to be composed of $^1/_8$ the minor component and $^7/_8$ the major component. The expected signal intensities from these atoms were then respectively $^1/_8$ and $^7/_8$ of the integral with respect to z, of eq 1, from 0 to ∞. In a packed powder of shell–core particles (Figure 1a), only the shell material is sampled in the first $1/2 r$ (dark line in Figure 1a). Since the overall mole ratio in the first layer is 7:1, the ratio of shell and core materials between $1/2 r$ and $4/3 r$ (light solid line in Figure 1a) must be 4:1. (An average thickness of $4/3 r$ for the first layer of particles was obtained by dividing the volume per particle by the projected area per particle.) Below the first layer, a uniform distribution was assumed. The contribution to the signal for the core material from atoms at these depths is $^1/_5$; i.e., the integral of eq 1 from $1/2 r$ to $4/3 r$ plus $^1/_7$ the integral from $4/3 r$ to ∞. Likewise, the signal from the shell material is expected to be the integral from 0 to $1/2 r$, i.e., $^4/_5$ the integral from $1/2 r$ to $4/3 r$ plus $^7/_8$ the integral from $4/3 r$ to ∞.

The signal intensity ratios (low- to high-energy electrons from the same atom) for the shell–core and unstructured samples are ratioed to eliminate the unknown I_0 terms. The mole fractions also cancel, eliminating the need to know the sample composition quantitatively. The amplification and attenuation factors cal-
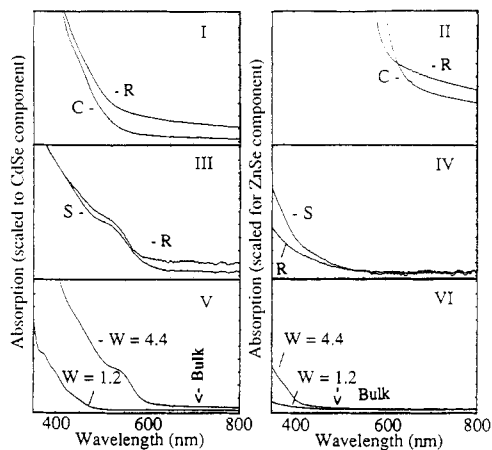
Figure 4. Absorption spectra illustrating core (C), random (R), or shell (S) components of the samples used in the XPS experiments and single material particles of the same size. The contribution of MSe to the particle's absorption is evaluated by comparing the absorbance per mole of MSe for particles in which it comprises the core, shell, major, or minor component to pure MSe particles the size of the core (W = 1.2) and overall particle (W = 4.4), with absorbance scaled to the molar extinction coefficient (roughly 0–1000 L M^{-1} cm^{-1}). CdSe components are shown in the left column and ZnSe components in the right. The top row illustrates the core material or minor component. Panel I: C = (ZnSe)$_7$CdSe, R = Zn$_7$CdSe. Panel II: C = (CdSe)$_7$ZnSe, R = Cd$_7$ZnSe$_8$. The middle row illustrates the shell material or major component. Panel III: S = (CdSe)$_7$ZnSe, R = Cd$_7$ZnSe$_8$. Panel IV: S = (ZnSe)$_7$CdSe, R = Zn$_7$CdSe$_8$. The spectra of capped single component CdSe and ZnSe particles: the size of the core (W = 1.2) and of the entire particle (W = 4.4) are shown in panels V and VI, respectively. The absorption onsets for bulk materials are also indicated by an arrow in panels V and VI.

Figure 5. Dependence of observed XPS and Auger signal attenuation or amplification on λ_b/λ_a of varying radii λ_a.

culated, using the assumptions above, for a 16-Å-radius (estimated from the micelle size) particle containing a uniform 8-Å shell are given in Table III. Values of λ calculated for ZnS[26] are used for this calculation. The experimental amplification and attenuation factors are also given in Table III. There is reasonable agreement between the experimental attenuation factors and those calculated.

The EDS experimental compositions reflect the fact that the thermodynamic driving force for the precipitation of CdSe is slightly higher than for ZnSe. This raises a question about how uniform the cation distribution is in the "unstructured" particles. Preference for the precipitation of CdSe may create a natural tendency toward CdSe-rich particle cores. Such a tendency would cause the observed amplification and attenuation factors for (ZnSe)$_7$CdSe/Zn$_7$CdSe$_8$ to be smaller, and those for (CdSe)$_7$ZnSe/Cd$_7$ZnSe$_8$ to be larger, than expected.

The absorption spectra of random and shell–core samples are shown in Figure 4. The top row shows the spectra of the samples for which CdSe, on the left, and ZnSe, on the right, are the core and minor components. The middle row shows the spectra for which CdSe, on the left, and ZnSe, on the right, are the shell and major components. The same spectra, scaled differently, are shown in panels I and IV and in panels II and III. The spectral scaling to extinction per mole of the component of interest was done to help determine the contribution of each component to the absorption spectra of the composite particles (as a function of structure).

The spectra of single material CdSe and ZnSe particles, with radii equal to the sample core and overall radii (W = 1.2 and 4.4), are shown in panels V and IV. In both cases, the optical absorption onsets of the small particles (W = 1.2 to a greater extent than W = 4.4) are blue-shifted from the bulk absorption onsets for these materials. These spectra are presented for comparison to the spectra of the layered particles to help discern the contribution of each component to the absorption spectra of the composite particles.

The fact that the core or minor component does not dominate the absorption spectra is seen by comparing the top and bottom rows. When a shell or major component of the particle is com-
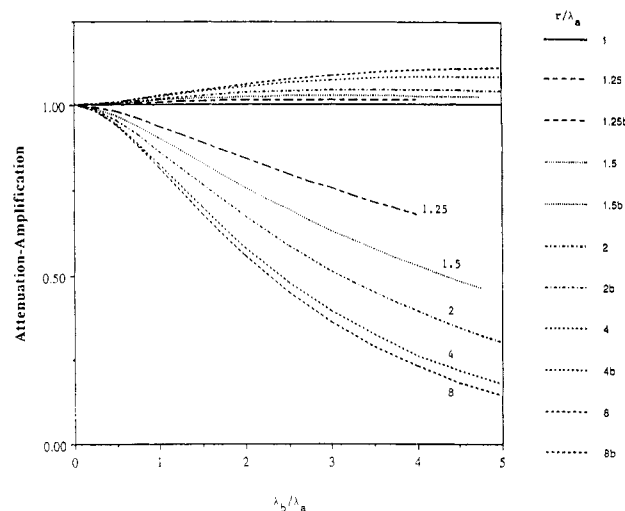
prised of the material with the lower bulk band gap, CdSe, the absorption spectrum is essentially the same as that of a pure CdSe particle of the same size (panels II and V). The presence of a CdSe core or minor component, however, shifts the absorbance onset of (ZnSe)$_7$CdSe and Zn$_7$CdSe$_8$ particles to the red of bulk ZnSe.

The spectra of the (CdSe)$_7$ZnSe and Cd$_7$ZnSe$_8$ samples in panel II bear no resemblance to the spectra of core-sized ZnSe particles, W = 1.2 in panel VI. When the same spectra are plotted scaled to the absorption due to the major component, CdSe, in panel III, these spectra look very much like the spectrum of CdSe W = 4.4 particles, panel V. There is no significant difference in the absorption spectra of the unstructured and shell–core type samples. Thus, there is no direct evidence in the absorption spectra to indicate particle structure. However, there is evidence that particles of CdSe did not nucleate separately and grow to the size of the micelles in the added micellar solution prior to the size equilibration of the micelle. If this were a significant process, the absorption onset in panel III would be at lower energy than the CdSe W = 4.4 onset in panel V.

The spectra of the (ZnSe)$_7$CdSe and Zn$_7$CdSe$_8$ samples are shown in panels I and IV. If these spectra were dominated by the absorption from their CdSe minor component, the traces in panel I would be similar to W = 1.2 in panel V. If they reflect instead mostly the absorption by the ZnSe major component, the traces in panel IV would resemble W = 4.4 in panel VI. The absorption of these particles is similar to that of W = 4.4 ZnSe particles but shifted to slightly lower energy by the presence of the CdSe. This shift indicates that the CdSe is incorporated in the ZnSe particles: that is, composite particles are indeed formed. The CdSe has essentially the same effect on the spectra of the particles when it is localized in the core and when it is distributed throughout the particle.

Summary

The preparation in micelles of small particles of either CdSe or ZnSe surrounded by a shell of the other material is reported. In the samples studied, the shell material dominates the optical properties of the particles, even when the narrower band gap material was used for the core. Nevertheless, absorption spectroscopy indicates that this preparation produces composite particles and not a mixture of single material particles. Our present level of precision in surface characterization does not allow us to differentiate small contributions in the minor species from a population with a lower W_1/W_2 core from a population which lacks the W_1 core. A comparison of the relative XPS and Auger signal intensities (for high- and low-energy electrons emitted by the same atomic species) from shell–core particles with those from particles with a random, constant spatial distribution is consistent with a nearly symmetrical layered shell–core structure in particles

obtained in the two-step preparation.

Appendix: Numerical Analysis of the XPS and Auger Intensity Data

The I_0 term in the expression for the depth dependence z of the observed signal intensity, eq 1, can be expanded

$$I = J_0 N(z)_i \sigma_i Y_{i,n} F(KE) e^{-z/\lambda(KE)} \qquad (A.1)$$

where J_0 is the X-ray flux, $N(z)_i$ is the number of i atoms, σ_i is the absorption cross section for atoms of i, $Y_{i,n}$ is the emission quantum yield for process n (XPS or Auger) for atoms of i, $F(KE)$ is the energy-dependent instrument response function, and $\lambda(KE)$ is the energy-dependent attenuation length for electrons traveling through the specific media.

In the special case where the emitting atom is uniformly distributed along the z axis, $N(z)_i$ is constant and eq A.1 can be integrated with respect to z to give

$$I_{int,i,n} = J_0 N_i \sigma_i Y_{i,n} F(KE) \, \lambda(KE) e^{-z/\lambda(KE)}|_0^\infty$$

$$I_{int,i,n} = J_0 N_i \sigma_i Y_{i,n} F(KE) \, \lambda(KE) \qquad (A.2)$$

The J_0, N_i, and σ_i terms cancel when the integrated intensity of two electrons emitted by the same atom are ratioed:

$$\frac{I_{int,i,a}}{I_{int,i,b}} = \frac{Y_{i,a} F(KE\,a) \, \lambda(KE\,a)}{Y_{i,b} F(KE\,b) \, \lambda(KE\,b)} \qquad (A.3)$$

Thus, for samples which have a uniform distribution of emitting atoms along the z axis, the ratio of the integrated signal intensities observed for two electrons emitted by the same type of atom is the ratio of the attenuation lengths of these electrons modified by the ratios of the emission quantum yields for the two processes and the instrument sensitivity to the two electrons. Since neither the emission quantum yields nor the instrument sensitivity changes for set processes in a given atom, the observed changes in the signal intensity ratios of the low- and high-energy electrons emitted by Cd and by Zn accompanying changes in the sample composition (Table II) must be due entirely to changes in the relative attenuation lengths of the two electrons.

The integration of eq A.1 is more complicated when the emitting atoms are not distributed uniformly along the z axis.

$$I_{int,i,n} = J_0 \sigma_i Y_{i,n} F(KE) \int N(z)_i e^{-z/\lambda(KE)} \qquad (A.4)$$

It is unlikely that eq A.4 could be integrated easily, even if the expression for $N(z)_i$ were known. Therefore, an approximation is made to simplify this integration. The sample is divided into three depth regions in which uniform atomic distributions are assumed. In a sample of perfect shell–core particles for which the shell thickness is $^1/_2$ the total particle radius, r, the surface

$1/2 r$ is always 100% shell material, regardless of how the particles are packed together. The average depth of the first layer of particles is equal to the volume per particle divided by the area per particle, $4/3 r$. The ratio of the shell and core materials in each particle is taken to be 7:1. In order to maintain this ratio through the first layer of particles, the ratio between $1/2 r$ and $4/3 r$ is taken as 4:1. The location of the point $z = 4/3 r$, at the end of the thin solid lines in Figure 1a, depends greatly on how the particles are packed. Very little need be said about this, however, since only a small percentage of the observed signal intensity comes from this deep in the sample. Thus, a uniform distribution of atoms with an atomic ratio of 7:1 is assumed at depths greater than $4/3 r$. For the shell material, eq A.2 becomes

$$I_{int,s,n} = J_0 \sigma_s Y_{s,n} F(KE)\{1 - \tfrac{1}{5} e^{-r/2\lambda_n} + (3/40) e^{-r/2\lambda_n}\} \qquad (A.5)$$

assuming that $N_s = 1$ from $z = 0$ to $1/2 r$, $^4/_5$ from $z = 1/2 r$ to $4/3 r$, and $^7/_8$ from $z = 4/3 r$ to ∞. For the core material, the same expression becomes

$$I_{int,c,n} = J_0 \sigma_c Y_{c,n} F(KE)\{\tfrac{1}{5} e^{-r/2\lambda_n} - (3/40) e^{-r/2\lambda_n}\} \qquad (A.6)$$

assuming that $N_c = 1$ from $z = 0$ to $1/2 r$, $^4/_5$ from $z = 1/2 r$ to $4/3 r$, and $^7/_8$ from $z = 4/3 r$ to ∞. Again, the J_0 and σ_i factors can be eliminated by ratioing the signal intensities of two electrons emitted by the same atom. $Y_{i,n}$ and $F(KE)$ can be eliminated by dividing these signal intensity ratios by the signal intensity ratios (A.3) obtained for the same atom in unstructured particles of the same composition. The resulting amplification (A.7) and attenuation (A.8) factors are

$$\frac{I_{int,s,a}}{I_{int,s,b}} = \frac{40 - 8e^{-r/2\lambda_a} + 3e^{-r/2\lambda_a}}{40 - 8e^{-r/2\lambda_b} + 3e^{-r-2\lambda_b}} \qquad (A.7)$$

$$\frac{I_{int,c,a}}{I_{int,c,b}} = \frac{8e^{-r/2\lambda_a} - 3e^{-r/2\lambda_a}}{8e^{-r/2\lambda_b} - 3e^{-r/2\lambda_b}} \qquad (A.8)$$

The attenuation and amplification factors obtained for particles with CdSe and ZnSe cores, using the calculated λ's for ZnS[26] and estimating the particles radius as 16 Å, are given in Table III. The calculated attenuation factors are in good agreement with those observed experimentally. However, the amplification factors are greatly underestimated by this model. Greater amplification factors can be obtained with this model by varying the proportionality constants between λ_a and λ_b, respectively the radii of the particle and core. The dependence of the amplification and attenuation factors calculated with this model for λ_b/λ_a is plotted for various particle radii/λ_a in Figure 5. While greater amplification factors are obtained when there is a greater difference between λ_a and λ_b and for larger particles, the observed values are not even approached. This shortcoming may be due in part to the failure of the model to take into account order below the first layer of particles and within the $1/2 r$ to $4/3 r$ region.